

Full Research Paper

Compound Cellular Imaging of Laser Scanning Confocal Microscopy by Using Gold Nanoparticles and Dyes

Shiao-Wen Tsai¹, Yi-Yun Chen¹ and Jiunn-Woei Liaw^{2,*}

¹ Institute of Biochemical and Biomedical Engineering, Chang Gung University 259 Wen-Hwa 1st Rd., Kwei-Shan, Tao-Yuan, 333, Taiwan; E-mail: swtsai@mail.cgu.edu.tw

² Department of Mechanical Engineering, Chang Gung University, 259 Wen-Hwa 1st Rd., Kwei-Shan, Tao-Yuan, 333, Taiwan; E-mail: markliaw@mail.cgu.edu.tw

* Author to whom correspondence should be addressed; E-mail: markliaw@mail.cgu.edu.tw

Received: 14 February 2008 / Accepted: 21 March 2008 / Published: 1 April 2008

Abstract: Combining the scattered light of gold nanoparticles (GNPs) and the fluorescence of dye molecules, a compound cellular imaging of laser scanning confocal microscopy (LSCM) is obtained. The human breast cancer cell line (MDA-MB-435S, BCRC 60429) is used for experiment. These cells are incubated with a glucose medium containing GNPs for 26 hours, and then are stained by Proidium Iodide (PI) for their nuclei. By using a single laser to illuminate these cells and adjusting the ranges of two bandpass filters for the detection, the scattered light from the GNPs and the fluorescence of PI can be induced simultaneously, but be detected separately without crosstalk. Furthermore, a compound cellular image can be obtained by merging the two images of the expressions of GNP and PI together. From the TEM images of these cells, it is observed that GNPs are aggregated in the vesicles of the cytoplasm due to the cell's endocytosis. The aggregation of GNPs makes the surface plasmon resonance band of GNPs broadened, so that strong scattered light from GNPs can be generated by the illumination of different-wavelength lasers (458, 488, 514, 561, and 633 nm).

Keywords: Cellular imaging, Gold nanoparticle, Laser scanning confocal microscopy, Surface plasmon resonance, Endocytosis, Light scattering.

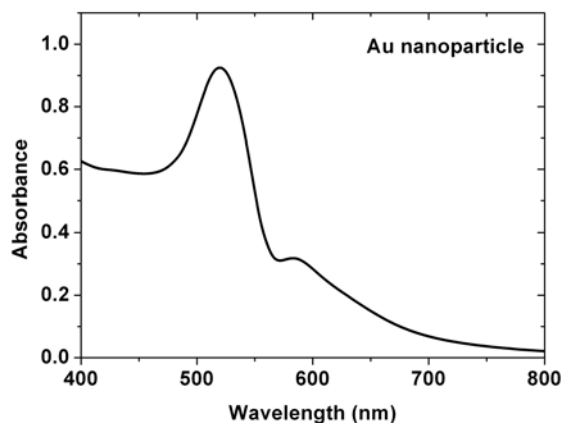
1. Introduction

The use of fluorescent dyes and fluorescent proteins as biomarkers becomes an important technique for cellular imaging of laser scanning confocal microscopy (LSCM) recently. A variety of dye molecules or proteins with different excitation and emission spectra were developed in the past decades. Combining different kinds of fluorophores and fluorescent proteins for staining the cells, a multi-fluorescence image of LSCM can be obtained by irradiating the sample with different-wavelength lasers. For example, the membrane, cytoplasm, mitochondria, and nucleus of a cell can be expressed individually by using different fluorescent dyes or proteins. However, because of the overlap of the emission spectra of different dyes, crosstalk could be caused sometimes for the multi-fluorescence. Therefore a data processing of unmixing is needed after the signal acquisition to separate these emission spectra from different biomarkers to interpret the signals. In addition, because of the photo-bleaching of dye molecules, it is not suitable for long-term observation by using fluorophores. In addition, the other new biomarkers [1], e.g., quantum dots (QDs) [2, 3] and metallic nanoparticles (MNPs) [4, 5], are also developed for cellular imaging recently. Since the mechanism of the emitted light from QD is the photoluminescence, the same with the dye-molecular fluorescence, the emission spectra of QDs are red-shifted from the excitation spectra, due to the Stokes shift. The advantage of QD lies in its narrow emission spectrum, high expression, and long-term observation. On the other hand, numerous researches have demonstrated the potential of MNPs as biomarkers, including gold nanoparticle (GNP) [6-8], porous GNP [9], gold nanorod [5, 10, 11], nanoshell [12], and nanocage [13] *etc.* Due to the surface plasmon resonance (SPR) of MNPs, which is a collective oscillation of electrons in the metal, a strong light scattering from MNPs can be induced when MNPs are irradiated by a light within a certain range of ultraviolet (UV) to near-infrared (NIR). Therefore, if a single-wavelength CW laser is used, the scattered light from MNPs is monochromatic and its wavelength is exactly the same with that of the laser. So far, some experiments have demonstrated the advantage of MNPs, bio-compatibility [14] and nontoxicity for cells [15, 16]. Moreover, surface functionalizing gold nanoparticles by the conjugation with a specific anti-body, e.g., anti-EGFR [8, 17] for epithelial cancer cell, has been developed for the applications of the diagnosis and the thermophoto-therapy of cancer cells [10, 12]. A darkfield imaging was also used to show the expression of the scattered light of GNPs from the membranes of cells [18], but not the signals from the cytoplasm. Except MNPs, using silver nanolayer to enhance fluorescence was proposed by using a total internal reflection fluorescence microscopy [19].

Although the techniques of using GNPs for the cellular imaging of LSCM were reported in some researches [8-11], a systematical study of GNP as biomarker for cellular imaging of LSCM by using different lasers, and a comparison of GNPs with fluorophores is still lacked for the extensive application. In this paper, we will demonstrate the feasibility of combining the images of GNP and dye for a compound cellular imaging of LSCM. The human mammary carcinoma cell line (MDA-MB-435S, BCRC 60429), which is a kind of human breast cancer cell, is used for tested. These cells are incubated with a glucose medium containing GNPs for 26 hours, and then stained by Proidium Iodide (PI) for their nucleuses. By using different-wavelength lasers (458, 488, 514, 561, and 633 nm) individually, strong scattered lights from GNPs and fluorescence of PI can be induced simultaneously. The two signals can be detected separately by using two bandpass filters. However, the emission of

dye PI can only be induced by the exciting laser with a wavelength shorter than 600 nm, so that no fluorescence of PI is detected by using laser of 633 nm.

Figure 1. The absorption spectrum of an aqueous solution of dispersed GNPs.



2. Preparation of Samples and Methods

2.1 Synthesis of GNP

For our experiments, GNPs are synthesized by using the seed-growth method [16]. The size of GNP is controllable by tuning the process of seed-growth method. For the following experiments, GNPs of a typical diameter of 30 nm are synthesized. Using the UV-vis-NIR spectrophotometer (Perkin Elmer Lambda 900), the absorption spectrum of an aqueous solution containing the dispersed GNPs is measured, as depicted in Figure 1. Since SPR is a collective oscillation of free electrons in a metallic nanoparticle, it will cause a strong scattering as well as absorption of light simultaneously. Therefore, the SPR band of GNP can be identified by using the absorption spectrum of dispersed GNPs. From Figure 1, the SPR band of GNP is from 400 nm to 600 nm, where the maximum SPR is at 520 nm.

2.2 Treatment of Cells

The cell for our experiment is the human mammary carcinoma cell line (MDA-MB-435S, BCRC 60429). In order to cause the GNP uptake by cells, these cells are incubated with a high-glucose medium containing GNPs of a specific optical density (OD) at 520 nm (the peak of SPR band). These GNPs are not modified by any surface conjugation, so that the uptake of GNPs by cells is only through the phagocytosis process, a kind of nonreceptor-mediated endocytosis. Normally, the uptake speed of nonreceptor-mediated endocytosis of cells is lower than that of receptor-mediated endocytosis [20]. Therefore the incubation time of cells with GNPs needs to be longer for cells taking up enough GNPs in the cytoplasm to have high expression of light scattering. After certain coculture time of cells with GNPs, sample is washed out the incubation medium, and RNase-solution is added to the sample for 20 min to remove the cytoplasmic RNA. Through the standard procedure, the nuclei of these cells can be stained by PI, because PI can bind with the nuclear RNA only.

Table 1. The ranges of two bandpass filters for different lasers; filter-I is for the scattered light from GNP and filter-II for the fluorescence of PI.

laser	458 nm	488 nm	514 nm	561 nm	633 nm
filter-I	443-561 nm	465-550 nm	497-561 nm	508-572 nm	615-647 nm
filter-II	604-668 nm	604-668 nm	604-668 nm	604-668 nm	604-630 nm

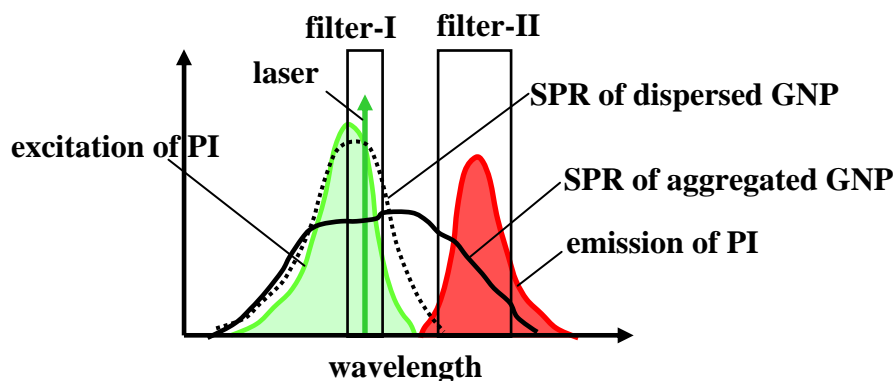
2.3 Lasers and Filters of LSCM

Three different lasers, Ar⁺ laser of 458/488/514 nm, diode pumped solid state (DPSS) laser of 561 nm, and He-Ne laser of 633 nm, are used to irradiate cells for LSCM (LSM 510 META, Zeiss) imaging. For each imaging, a single laser is used to irradiate the sample, and two corresponding bandpass filters are set to separate the scattered light from GNP and the fluorescence of PI, as listed in Table 1, where filter-I allows the scattered light to pass and filter-II for the fluorescence. The schematic diagram of the two filters is depicted in Figure 2. Concerning the setting of the ranges of the two bandpass filters, the excitation and emission spectra of PI as well as the wavelength of laser need to be taken into account. The SPR band of GNP is from 400 to 600 nm. Therefore, if wavelength of the laser is within the SPR range, the scattered light from GNPs can be generated, which is monochromatic, and the wavelength is the same with the single-wavelength laser. On the other hand, the excitation band of PI is from 450 nm to 600 nm, where the maximum excitation occurs at 535 nm, and the emission band of PI is from 585 nm to 720 nm, where the maximum emission of fluorescence is at 620 nm. Therefore, only when the wavelength of laser is within the excitation spectrum of PI, the fluorescence can be induced, whose emission spectrum is always red-shifted from the wavelength of the exciting laser, due to the Stokes shift. Summarily, the range of filter-I is set to cover the wavelength of a specific laser only for the detection of the scattered light from GNPs, but to reject the emission band of PI. In contrast, the range of filter-II is set to be 604-668 nm, which covers the emission of PI but reject the scattered light from GNP for all lasers, except for the He-Ne laser of 633 nm. For He-Ne laser of 633 nm, filter-II is set to be 604-630 nm to avoid the contamination from the scattered light of 633 nm. With the aid of the two filters, two cellular images are acquired individually. Since no overlap is between the ranges of the two filters, no crosstalk is caused in the two images. Furthermore, a compound image is obtained by merging the two images. In addition, using a pinhole, the out-of-focus signals are rejected, so the optical section image of the focal plane can be obtained. The size of the confocal pinhole is set to be 1.12 and 1.3 Airy units for PI and GNP, respectively.

Since the maximum excitation of PI is at 535 nm and the peak of SPR band of aggregated GNP could be at 540 nm, the best candidates are green-light lasers, e.g., Nd-YAG laser of 532 nm, He-Ne laser of 543 nm, and DPSS laser of 561 nm etc. However, for the other lasers, if their wavelengths are within the range of the excitation band of PI (450-600 nm), the fluorescence of PI still can be induced, but a higher power of the laser is needed to obtain enough fluorescence expression. In our LSCM, there are a reflection grating to disperse the collected light evenly and a 32-PMT (photomultiplier tube) array

for detecting different wavelength lights. This design provides us a feasibility to set the upper and lower cut-off frequencies of these bandpass filters by software.

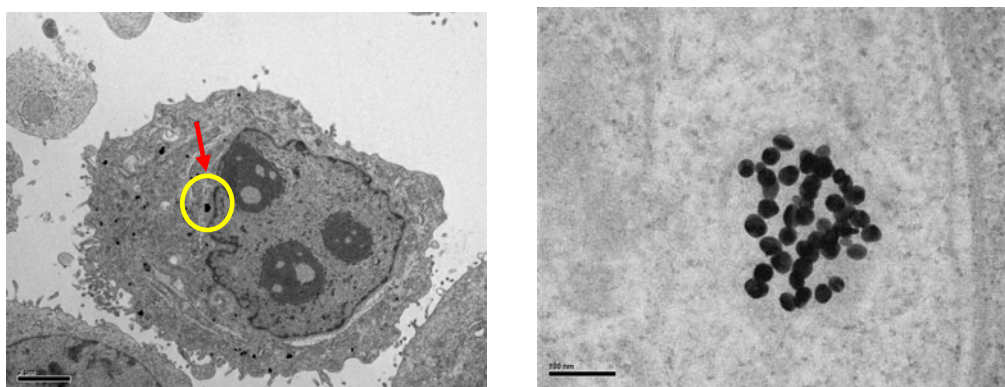
Figure 2. The schematic diagram of the ranges of two bandpass filters related to the excitation and emission spectra of dye (PI), the SPR band of GNP, and the wavelength of laser. The dashed black line denotes the SPR band of dispersed GNPs, and the solid black line denotes the SPR band of aggregated GNPs.



3. Experimental Results & Discussion

3.1 Image of TEM

Figure 3. Transmission electron microscope images of MD-MBA-435S cells treated with GNP for 24 hours. A) The image of the cell (x5000), where the scalar bar is 2 μm , shows the internalization of GNRs by the cell. B) An image of higher magnification (x150000) at the marked location shows the uptake of GNP in cellular vesicle, where the scale bar denotes 100 nm.



3A 3B

A sample of MD-MBA-435S cells was incubated with a glucose medium containing GNPs (OD=0.5 at 520 nm) for 24 hours, and then was prepared for TEM imaging, as shown in Figure 3. The high-magnification TEM image (x150000) shows that these GNPs are aggregated in the vesicles in the cytoplasm [15], rather than attach on the membrane only, as shown in Figure 3B. The aggregation is due to the GNPs uptake by these cells through the endocytosis process. This is because that when

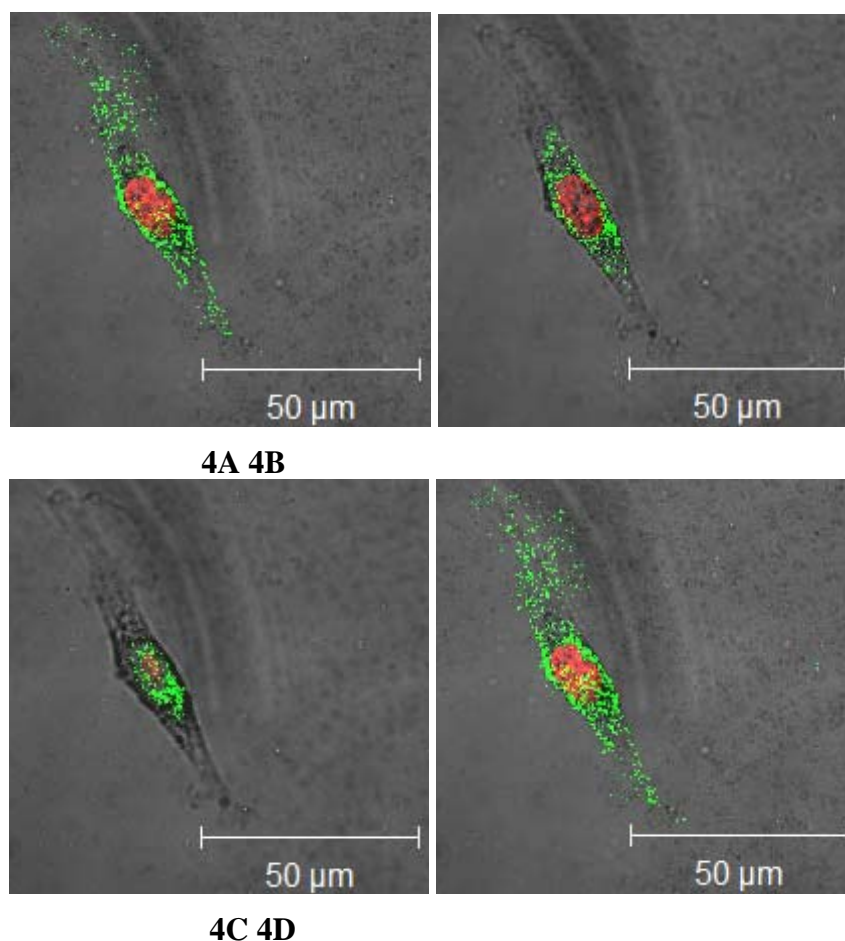
some gold nanoparticles adhere to cell's membrane, the membrane is stimulated to form a small pocket locally around these gold nanoparticles to enclose them gradually. Therefore, these gold nanoparticles are aggregated in the closed pocket (vesicle) finally, when they are internalized. The diameter distribution of these vesicles is about 200-300 nm. In each vesicle, certain numbers of GNPs are enclosed. The averaged diameter of GNP is about 30 nm. Actually, a normal human breast cell line was also studied by using the above same procedure. A same phenomenon of clustered GNPs in vesicles was also observed in the normal cells. Since these GNPs are not treated by any surface functionalization, they do not possess a specific antireceptor to link with specific receptor. Therefore, GNP is not selective for the endocytosis of different cells. For our experience, the uptake speeds of GNPs by the normal breast cells and MD-MBA-435S cells are almost the same.

3.2 Images of LSCM

For LSCM imaging, another sample of MD-MBA-435S cells incubated with a glucose medium containing GNPs (OD=1.1 at 520 nm) for 26 hours was also prepared. To make sure that no contamination from the autofluorescence of cells themselves, two control groups were prepared and measured in advance by using the same conditions of Table I for LSCM imaging; one is MD-MBA-435S cell without treatments of GNP and PI, and the other is MD-MBA-435S cell stained by PI. For the first control group, no any signal is detected for both filters, and for the second one, only the fluorescence of PI is detected from the nucleus. The size of the confocal pinhole is set to be 1.12 and 1.3 Airy units for PI and GNP, respectively. The optical-section images at different depths are obtained by changing the focal plane of LSCM. The compound images of the scattered light and fluorescence by using DPSS laser of 561 nm at different depths, from the bottom (0 μm), middle (2 μm), to top (4 μm) of cells, are shown in Figures 4A, 4B, and 4C, respectively. Each compound image is colorized by two pseudo-colors, according to the ranges of filter-I and filter-II, where the red area is the expression of PI from the nucleus, and these discrete green lightspots are the expressions of GNPs in the cytoplasm. Each lightspot is the scattered light from a cluster of GNPs in a vesicle. Moreover, these optical-section images indicate that GNPs are uniformly distributed in the cytoplasm. The three-dimensional projection, as shown in Figure 4D, is obtained by merging Figures 4A, 4B and 4C. In these figures, the image of transmitted light is also merged. Normally, the pinhole size, P , controls the effective thickness d of the optical section imaging; i.e., the z -axis resolution d is proportional to the value of $Pn\lambda/(N.A.)^2$, where n is the refractive index of the immersion medium, λ is the wavelength of signal, and $N.A.$ is the numerical aperture of object lens. On the other hand, the lateral resolution R_L of LSCM is $0.4\lambda/(N.A.)$, and the diffraction-limited spot size of the focused laser beam is $0.5\lambda/n_s$, where n_s is the refractive index of sample. For example, if $P=1.3$ Airy units, $n=1.518$ (Zeiss immersion oil), $\lambda=561$ nm, and $N.A.=1.4$ (magnification is 63), the z -axis resolution is $d=565$ nm, the lateral resolution is $R_L=160$ nm, and the diffraction-limited spot size is 210 nm for $n_s=1.33$ (in water). A scan resolution of 1024x1024 pixels is used to acquire the LSCM images, where each pixel size is around 232 nm. In order to obtain enough scattered signals for imaging, the dwell time (pixel time) should be chosen properly. If the distance of two adjacent vesicles containing GNPs is larger than the lateral resolution, they can be distinguished from each other in x - y plane, where the diameter of a vesicle is about 250 nm. Actually the scattering cross section of a metallic nanoparticle is larger than its real size, because

of the SPR. However, the z-axis resolution is larger than the diameter of a vesicle, so that some out-of-focus scattered lights of GNPs could be detected. Therefore, a few of green lightspots are still observed in the nucleus, which actually result from the scattered lights from some vesicles beneath but very close to the nucleus, as shown in the bottom cellular image of Figure 4A. In contrast, no lightspot is indicated in the nucleus, as shown in the middle optical section of cellular image of Figure 4B. In fact, according to our experience of TEM imaging, no GNPs inside the nucleus are observed as far. A spindle shape of the cell is observed, because the cell adheres on the substrate.

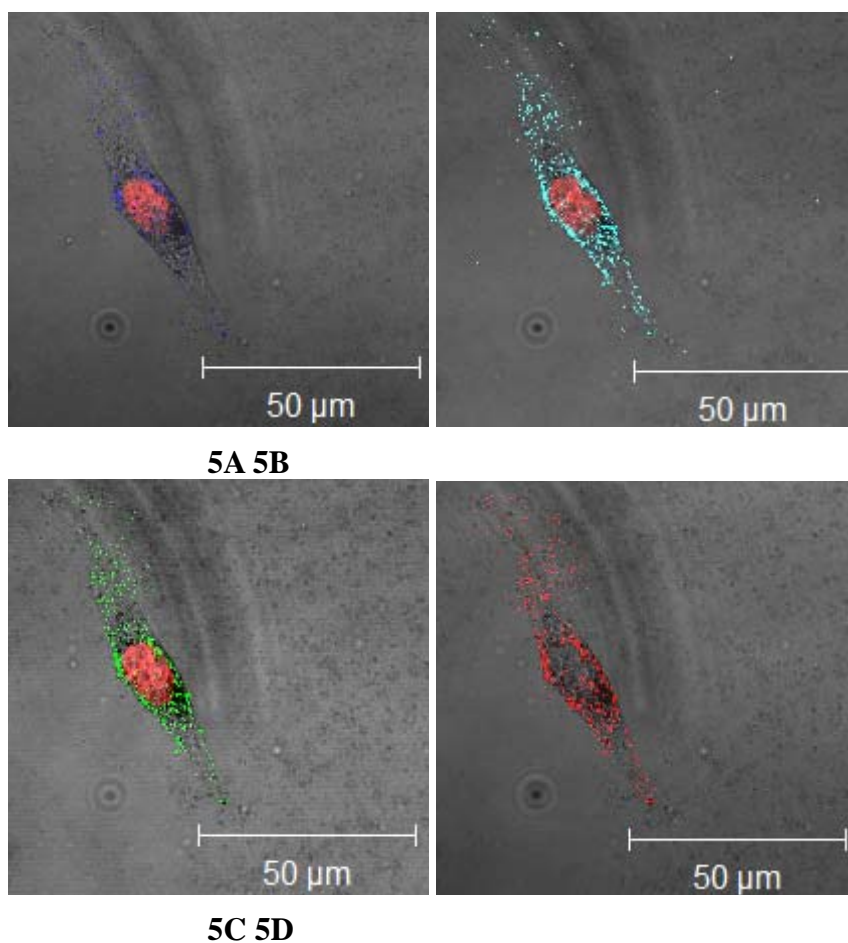
Figure 4. The LSCM images by DPSS laser of 561nm at different depths; A) bottom, B) middle, C) top, and D) 3D projection.



Furthermore, the compound images of 3D projection by other lasers (458, 488, 514, and 633 nm) are shown in Figures 5A, 5B, 5C, and 5D, respectively, at the same location of the sample as Figure 4. Since the wavelengths of these lasers (458, 488, and 514 nm) are also within both the excitation band of PI and the SPR band of GNP, both the fluorescence from PI and the scattered light from GNP can be induced simultaneously, but their expressions are relatively weaker than that of DPSS laser. The phenomena are attributed to the broadened SPR band of GNPs caused by the aggregation of GNPs in vesicles [21]. Hence the strong light scattered from GNPs can also be induced by using different-wavelength lasers, rather than green-light laser only. Moreover the maximum SPR of the aggregated GNPs could be little red-shifted from that of the dispersed GNPs (520 nm), as shown in Figure 2.

Therefore, DPSS laser of 561 nm is the optimal option for generating the scattered light from GNPs and the fluorescence of PI simultaneously. Comparing the expressions of GNP and PI of different lasers, both the expressions of the fluorescence of PI and the scattered light of GNP by using DPSS laser (561 nm) are indeed stronger than the other lasers. As to He-Ne laser of 633 nm, although it can also induce the scattered light from GNP (the peak SPR is at 520 nm), its wavelength is too long to excite PI for emitting fluorescence; i.e., the wavelength of 633 nm is out of the excitation band of PI. Since PI can not be excited by the illumination of He-Ne laser of 633 nm, no fluorescence is detected. Therefore, a dark area is observed at the nucleus without the expression of PI, but a bright zone with numerous red lightspots in the cytoplasm resulting from the scattering light of GNPs is still observed from the compound image of He-Ne laser (633 nm), as shown in Figure 5D. Moreover, several samples were incubated with media containing GNPs of different OD values for different culture times, and then were also measured by LSCM. We found that normally the higher the OD value, the higher the expression of GNPs in the cellular image. In addition, the longer the culture time of cells with the glucose medium, the more the uptake of GNPs by the cells.

Figure 5. 3D projection compound cellular images by using different lasers, A) 458 nm, B) 488 nm, C) 514 nm, and D) 633 nm.



4. Conclusion

In this paper, we have demonstrated how to combine the scattered light from GNPs and the fluorescence of dye (PI) for a compound cellular imaging of LSCM, where the human breast cancer cell line (MDA-MB-435S) is tested. For LSCM measurement, two signals are generated simultaneously by a single laser, and can be separately detected by using two bandpass filters of different ranges. The scattered light is reflected from the GNPs in the vesicles in the cytoplasm, and the fluorescence is emitted from the dye (PI) in the nuclei. The scattered light is monochromatic, and the wavelength is the same with the illuminating CW laser. In contrast, the spectrum of the fluorescence of dye is red-shifted from the wavelength of the laser. Therefore, there is no crosstalk between the two signals. According to the wavelength range of the two filters, two pseudo-colors are used respectively for the two images of the scattered light and fluorescence, and then they can be merged to be a compound image. Consequently, the compound cellular image of LSCM provides more information or fingerprint by combining the two biomarkers (GNPs and dyes). In the future, multiple targeted probes (e.g., fluorescent dyes, QDs, GNPs) can be mixed for use and illuminated by multiple lasers for obtaining versatile cellular imaging. Since the SPR band of MNPs is dependent of their shape, one of the advantages of using MNPs as biomarker is to tune the wavelength of the maximum scattering on demand by changing their shape and size. Moreover, each probe can be surface functionalized with specific bioconjugation to be a ligand-linking biomarker [22, 23].

Acknowledgements

We acknowledge the assistance of Prof. Fu-Yin Hsu, National Taiwan Ocean University, in cell's staining of PI. This research was supported by National Science Council, Taiwan, R.O.C. (Grant NSC 95-2221-E-182-044 and NSC 94-2213-E-182-024).

References and Notes

1. Santra, S.; Dutta, D.; Walter, G.A.; Moudgil, B.M. Fluorescent nanoparticle probes for cancer imaging. *Tech. Cancer Res. Treat.* **2005**, *4*, 593-602.
2. Larson, D.R.; Zipfel, W.R.; Williams, R.M.; Clark, S.W.; Bruchez, M.P.; Wise, F.W.; Webb, W.W. Water-soluble quantum dots for multiphoton fluorescence imaging in vivo. *Science* **2003**, *30*, 1434-1436.
3. Jaiswal, J.K.; Mattoussi, H.; Mauro, J.M.; Simon, S.M. Long-term multiple color imaging of live cells using quantum dot bioconjugates. *Nature* **2003**, *21*, 47-51.
4. Schultz, S.; Smith, D.R.; Mock, J. J.; Schultz, D.A. Single-target molecule detection with nonbleaching multicolor optical immunolabels. *Proc. Natl. Acad. Science* **2000**, *97*, 996-1001.
5. Wang, H.; Huff, T.B.; Zweifel, D.A.; He, W.; Low, P.S.; Wei, A.; Cheng, J.X. In vitro and in vivo two-photon luminescence imaging of single gold nanorods. *Proc. Natl. Acad. Science* **2005**, *102*, 15752-15756.
6. Sokolov, K.; Aaron, J.; Hsu, B.; Nida, D.; Gillenwater, A.; Follen, M.; MacAulay, C.; Adler-Storthz, K.; Korgel, B.; Descour, M.; Pasqualini, R.; Arap, W.; Lam, W.; Richards-Kortum, R.

- Optical systems for in vivo molecular imaging of cancer. *Tech. Cancer Res. Treat.* **2003**, *2*, 491-504.
7. Sokolov, K.; Follen, M.; Aaron, J.; Pavova, I.; Malpica, A.; Lotan, R.; Richards-Kortum, R. Real-time vital optical imaging of precancer using anti-epidermal growth factor receptor antibodies conjugated to gold nanoparticles. *Cancer Res.* **2003**, *63*, 1999-2004.
 8. El-Sayed, I.H.; Huang, X.; El-Sayed, M.A. Surface plasmon resonance scattering and absorption of anti-EGFR antibody conjugated gold nanoparticles in cancer diagnostics: Applications in oral cancer. *Nano Lett.* **2005**, *5*, 829-834.
 9. Shukla, S.; Priscilla, A.; Banerjee, M.; Bhonde, R.R.; Ghatak, J.; Satyam, P.V.; Satry, M. Porous gold nanoparticles by controlled transmetalation relation: a novel material for application in cell imaging. *Chem. Matter.* **2005**, *17*, 5000-5005.
 10. Huang, X.; El-Sayed, I.H.; Oian, W.; El-Sayed, M.A. Cancer cell imaging and photothermal therapy in the near-infrared region by using gold nanorods. *J. Am. Chem. Soc.* **2006**, *128*, 2115-2120.
 11. Chen, C.C.; Lin, I.P.; Tzeng, S.C.; Wang, J.W.; Wu, C.H.; Chen, Y.C.; Chen, J.P.; Chen, K.H.; Su, M.T.; Wu, Y.C. DNA-gold nanorod conjugates for remote control of localized gene expression by near infrared irradiation. *J. Am. Chem. Soc.* **2006**, *128*, 3709-3715.
 12. Loo, C.; Lowery, A.; Halas, N.; West, J.; Drezek, R. Immunotargeted nanoshells for integrated cancer imaging and therapy. *Nano Lett.* **2005**, *5*, 709-711.
 13. Chen, J.; Saeki, F.; Wiley, B.J.; Cang, H.; Cobb, M.J.; Li, Z.-Y.; Au, L.; Zhang, H.; Kimmey, M. B.; Li, X.; Xia, Y. "Gold nanocages: bioconjugation and their potential use as optical imaging contrast agents" *Nano Lett.* **2005**, *5*, 473-477.
 14. Shukla, R.; Bansal, V.; Chaudhary, M.; Basu, A.; Bhonde, R. R.; Sastry, M. Biocompatibility of gold nanoparticles and their endocytotic fate inside the cellular compartment: A microscopic overview. *Langmuir* **2005**, *21*, 10644.
 15. Chithrani, B.D.; Ghazani, A.A.; Chan, W.C.W. Determining the size and shape dependence of gold nanoparticle uptake into Mammalian cells. *Nano Lett.* **2006**, *6*, 662-668.
 16. Yang, P.-H.; Sun, X.; Chiu, J.-F.; Sun, H.; He, Q.-Y. Transferrin-mediated gold nanoparticle cellular uptake. *Bioconjugate Chem.* **2005**, *16*, 494-496.
 17. Aaron, J.; Oh, J.; Larson, T.A.; Kumar, S.; Milner, T.E.; Sokolov, K. Increased optical contrast in imaging of epidermal growth factor receptor using magnetically actuated hybrid gold/iron oxide nanoparticles. *Opt. Express* **2006**, *14*, 12930-12943.
 18. Curry, A.; Hwang, W.L.; Wax, A. Epi-illumination through the microscope objective applied to darkfield imaging and microspectroscopy of nanoparticle interaction with cells in culture. *Opt. Express* **2006**, *14*, 6535-6542.
 19. He, R.-Y.; Chang, G.-L.; Wu, H.-L.; Lin, C.-H.; Chiu, K.-C.; Su, Y.-D.; Chen, S.-J. Enhanced live cell membrane imaging using surface plasmon-enhanced total internal reflection fluorescence microscopy. *Opt. Express* **2006**, *14*, 9307-9316.
 20. Zhang, Y.; Kohler, N.; Zhang, M. Surface modification of superparamagnetic magnetite nanoparticles and their intracellular uptake. *Biomaterials* **2002**, *23*, 1553-1561.

21. Ngoc Bui, M.-P.; Baek, T.J.; Seong, G.H. Gold nanoparticle aggregation-based highly sensitive DNA detection using atomic force microscopy. *Anal. Bioanal. Chem.* **2007**, *388*, 1185-1190.
22. Patra, H.K.; Banerjee, S.; Chaudhuri, U.; Lahiri, P.; Dasgupta, A.K. Cell selective response to gold nanoparticles. *Nanomedicine* **2007**, *3*, 111-119.
23. Aaron, J.; Nitin, N.; Travis, K.; Kumar, S.; Collier, T.; Park, S.Y.; Jose-Yacaman, M.; Coghlan, L.; Follen, M.; Richards-Kortum, R.; Sokolov, K. Plasmon resonance coupling of metal nanoparticles for molecular imaging of carcinogenesis in vivo. *J. Biomedical Optics* **2007**, *12*, 034007.

© 2008 by MDPI (<http://www.mdpi.org>). Reproduction is permitted for noncommercial purposes.